Solar Energy Materials and Solar Cells 174 (2018) 7–15

Contents lists available at ScienceDirect

Solar Energy Materials and Solar Cells

journal homepage: www.elsevier.com/locate/solmat

Mechanical stability of roll-to-roll printed solar cells under cyclic bending and torsion

Mickey Finn III[a], Christian James Martens[a], Aliaksandr V. Zaretski[a], Bérenger Roth[a,b], Roar R. Søndergaard[b], Frederik C. Krebs[b,*], Darren J. Lipomi[a,*]

[a] Department of NanoEngineering, University of California, San Diego 9500 Gilman Drive, Mail Code 0448, La Jolla, CA 92093-0448, United States
[b] Department of Energy Conversion and Storage, Technical University of Denmark, Frederiksborgvej 399, DK-4000 Roskilde, Denmark

ARTICLE INFO

Keywords:
Organic solar cell
Conjugated polymer
Flexible electronics
Barrier encapsulation
Mechanical stability
Cyclic fatigue testing

ABSTRACT

The ability of printed organic solar cells (OSCs) to survive repeated mechanical deformation is critical to large-scale implementation. This paper reports an investigation into the mechanical stability of OSCs through bending and torsion testing of whole printed modules. Two types of modules are used that differ slightly in thickness as well as on the basis of the electrode materials: silver nanowires or carbon-based inks. Each type of module is subjected to two different mechanical modes of deformation, bending and torsion, of several thousand cycles per module using a purpose-built robotic device. Analysis of the distribution of stress in the devices performed by finite-element modeling predicts the locations of failure. Failure upon bending originates at the laser-cut edges of the modules from shear at the clamp/module interface leading to crazing of the plastic barrier encapsulant foils. This crazing leads to eventual delamination due first to decohesion of the active layer at the edge of the modules and later to deadhesion between the PEDOT:PSS (electrode) and P3HT:PCBM (semiconductor) layers. The torsion mode imposes greater stresses than the bending mode and thus leads to failure at fewer strain cycles. Failure during torsion occurs through crack propagation initiated at stress concentrations on the edges of the module that were imposed by their rectangular geometry and ultimately leads to bifurcation of the entire module. Rather than the differences in electrode materials, the differences in survivability between the two types of modules are attributed mostly to the thickness of the substrate materials used, with the thinner substrate used in the carbon-based modules (~160 μm) failing at fewer strain cycles than the substrate used in the silver-nanowire-based modules (~190 μm). Taken together, the results suggest ways in which the lifetimes of devices can be extended by the layouts of modules and choices of materials.

1. Introduction

Mechanical flexibility is the characteristic that enables most of the advantages of printed modules based on organic semiconductors [1]. In particular, organic solar cells (OSCs) must survive the rigors of roll-to-roll coating, use in the outdoor environment (e.g., exposure to the forces of wind, rain, and snow), and diurnal and seasonal changes and concomitant thermal expansion and contraction [2]. Portable applications in particular expose the modules to the most extreme modes of mechanical insult, including impact, shear, twisting, stretching, bending, and folding [3]. For modules to accommodate these types of deformations, the substrates, encapsulants, and active materials must act in concert to store or dissipate mechanical energy in ways that do not degrade the electronic performance. Despite considerable research into the understanding of the mechanical properties of their component materials and the adhesion between individual device layers [1,4–7], the stability of whole modules against cyclic (repeated) deformations has not been reported. This study investigates the decline in performance (and eventual failure) of packaged solar modules after thousands of repeated cycles with a stress amplitude below the yield stress of the component materials. In particular, two different types of devices were used and subjected to two different modes of deformation: bending and torsion. These modes were meant to mimic the types of deformations that might be encountered during the real-world operation of devices.

2. Background

Organic solar cells have been the subject of intense research over the last decade due to the low cost, low weight, mechanical compliance and scalability that comes with thin-film solution processing methods

* Corresponding authors.
E-mail addresses: frkr@dtu.dk (F.C. Krebs), dlipomi@ucsd.edu (D.J. Lipomi).

http://dx.doi.org/10.1016/j.solmat.2017.08.015
Received 13 June 2017; Received in revised form 7 August 2017; Accepted 11 August 2017

such as inkjet printing and roll-to-roll manufacturing [8]. Although OSCs employing a wide range of conjugated polymers as the active layer are less efficient than devices based on conventional inorganic semiconductors, lab scale devices with power conversion efficiencies (*PCE*) greater than 10% have been reported [9,10]. Such efficiencies are more than sufficient for use in an array of portable applications, such as power sources for wearable biosensors, consumer electronics, and LED lighting [11,12]. One can visualize a future in which ultrathin and inexpensive portable electronics are powered by flexible printed solar cells, provided such devices are mechanically compliant enough to withstand prolonged usage.

The majority of investigations into the mechanical stability of OSCs has focused on the elasticity of the conjugated polymer used as the active layer [13], as well as electrode materials such as poly(3,4-ethylenedioxythiophene): poly(styrene sulfonate) (PEDOT:PSS) [14]. Such investigations, however, have focused on determining mechanical properties (e.g., elastic modulus or crack onset strain) of single component films [15–17]. Other forms of micromechanical testing, such as the single cantilever beam method, have been employed to study the cohesion of individual module layers while the four-point bending method and double cantilever method have been employed to study the adhesion at the interface between device layers [18–20]. While mechanical characterization of materials in isolation is now well developed, work on whole devices has lagged behind, with few exceptions [6]. In particular, the long-term durability of whole OSC modules under repeated elastic strains has not been reported.

3. Experimental design

3.1. Selection of OSC modules

The modules tested in this study (Fig. 1) were roll-to-roll printed in open air by the group of Frederick Krebs at the Danish Technical University and are described in great detail elsewhere [21,22]. We chose two types of modules. The primary differences between the two types were the use of carbon-based inks versus silver nanoparticle ink for the serial electrode links between the individual photocells that make up the modules. In the carbon electrode (C-type) module, the device stack had the configuration PEDOT:PSS/ZnO/P3HT:PCBM/PEDOT:PSS. In this configuration, the ZnO is a hole-blocking layer that permitted the use of PEDOT:PSS as both the cathode and anode. In the silver electrode (Ag-type) modules, the PEDOT:PSS used as a cathode was replaced by a hybrid blend of ZnO and silver nanowires (AgNW) to form the configuration AgNW:ZnO/P3HT:PCBM/PEDOT:PSS. Aside from these differences in the selection of materials, an important additional difference was the use of a UV filter in addition to the barrier foil for the Ag-type module [22,23]. Encapsulation in both cases was provided by Amcor Ceramis, a commercially available multilaminate barrier foil consisting

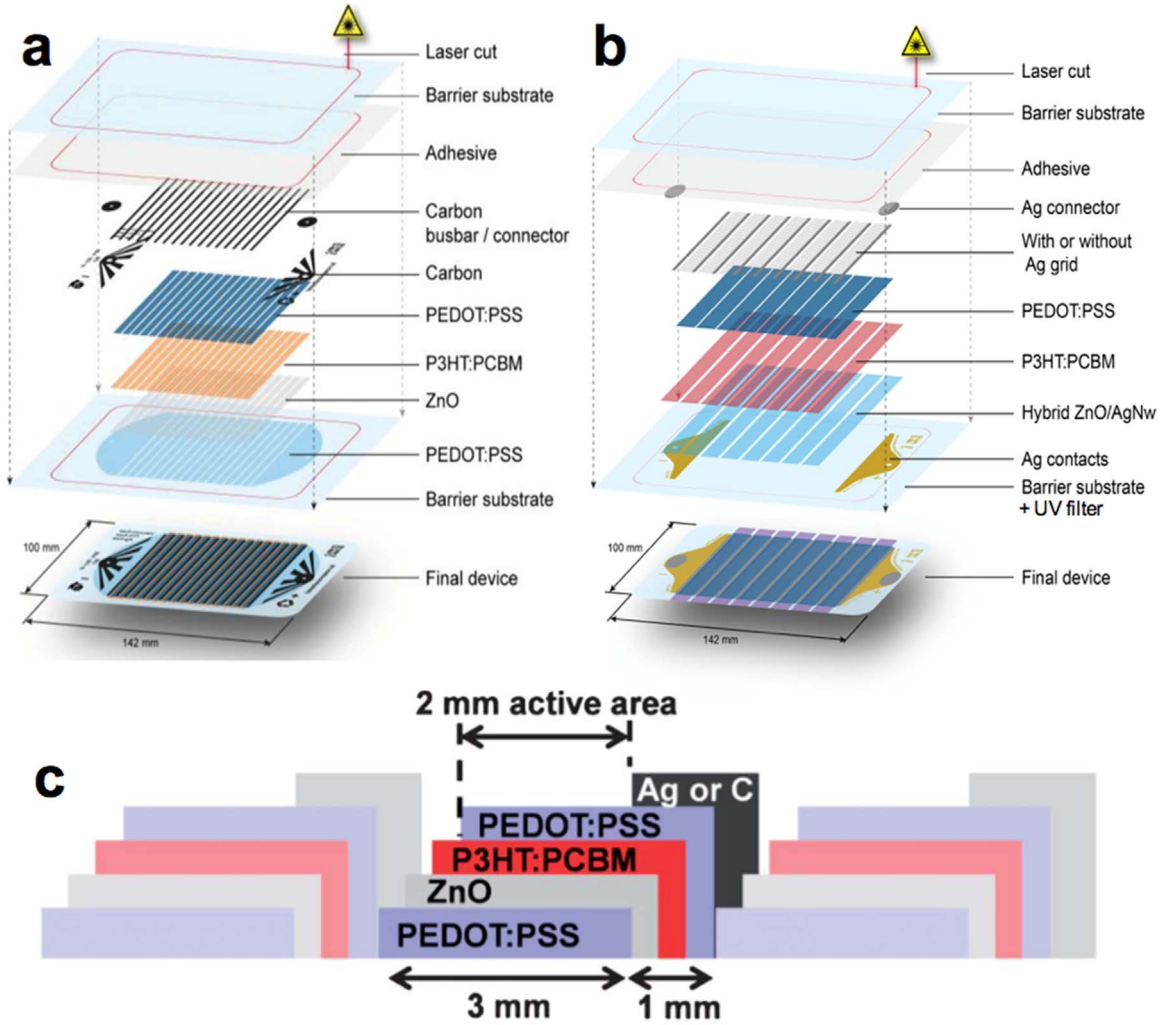

Fig. 1. Schematic diagrams of (a) C-type and (b) Ag-type module. (c) Cross sectional schematic diagram of the module stack illustrating the serial electrical connectivity within the module. (a) And (b) reproduced with permission from Ref. [24]. Copyright 2015, Wiley-VCH Verlag, GmbH & Co., KGaA. (c) reproduced with permission from Ref. [25]. Copyright 2012, Royal Society of Chemistry.

of 12 μm layers of biaxially oriented poly(ethylene terephalate) (oPET) alternating with 40–80 nm layers of evaporated silicon dioxide. The PEDOT:PSS layers were both rotary screen printed at a web speed of 10 m min^{-1} for the first highly conductive layer and 4 m min^{-1} for the thinner back layer and were both dried by traveling through ovens set to 90 °C and 140 °C. Both the active layer and the ZnO layer were slot-die coated at a web speed of 2 m min^{-1} and dried with both ovens at 140 °C. The UV-curable adhesive that enabled encapsulation was DELO Katiobond LP655 applied by flexo-printing where the adhesive was applied to the back barrier foil with the front barrier foil and device stack used as the laminate. After being run through a nip at < 1 m min^{-1} that laminated the two films, they traveled at 2 m min^{-1} under a 2 kW UV lamp followed by a 350 W LED curing lamp. After lamination, individual modules were cut into sections from the 305 mm wide parent roll with the use of a 90 W CO_2 laser at a web speed of 4.5 m min^{-1}. The thickness measured at the outside edge of each device was approximately160 μm for the C-type and 190 μm for the Ag-type modules due to the additional UV filter.

3.2. Analytical determination of testing parameters

Bending and torsion were chosen as the mechanical modes for this study in order to investigate the behavior of the devices under expansion, compression, and shear. We reasoned that bending and torsion are types of deformation that would be encountered during the fabrication and installation of modules, and would be encountered ubiquitously in outdoor operation of modules. Specifically, large-area OSC films deployed in the field might become unfastened over time, and depending on the angle of incident gusts of wind, might experience both bending and shear repeatedly. Such thin film OSC modules could conceivably endure thousands of bending and torsion cycles in the course of a night spent undulating like a sail in the wind. Similarly, OSC employed to power wearable sensors and consumer electronics must be able to withstand both repeated application and the wide range of motion that conformal contact with the human body requires. The object of this study was to test the effects of fatigue and wear under cyclic loading of the active materials, along with the barrier foils. In order to design our testing apparatus and parameters to produce stresses that would not immediately deform the oPET substrate and thus cause catastrophic failure of the modules on the first deformation, we determined the parameters analytically (see Supporting Information for details). In summary, we designed an apparatus for torsion that produced a maximum shear stress of 1.4 MPa, well below the yield strength of 100 MPa for the polymeric component of the barrier material, oPET.

3.3. Design of mechanical apparatus

To implement normal bending strain on the OSC modules, we constructed a robotic apparatus (Fig. 2). The apparatus gripped both ends of the modules using slabs of poly(dimethylsiloxane) (PDMS) that were clamped with aluminum bars. The apparatus was configured to keep one end of the solar cell fixed while moving the other end in an arc so that a bend occurred approximately at the transverse midplane between the clamped ends. The testing apparatus was limited to a minimum radius of curvature of 8 mm by the range of motion of the fixed arm (see Video V1). Due to this constraint, the maximum strain at the apex of the bend was found to be approximately 1% for the C-type modules and 1.2% for the slightly thicker Ag-type modules. This strain was tensile on the convex surface of the bend and compressive on the concave surface of the bend.

For testing shear, the apparatus was modified to produce torsion. We suspected that the twisting motion would damage the devices after fewer cycles than the bending motion so that the decline in performance would occur more readily. Using analytical relations from classical mechanics along with measured rotational displacement, it was possible to understand the shear stress experienced by the tested samples (see Supporting Information). This analysis was complicated, however, by the presence of the springs that were necessary to

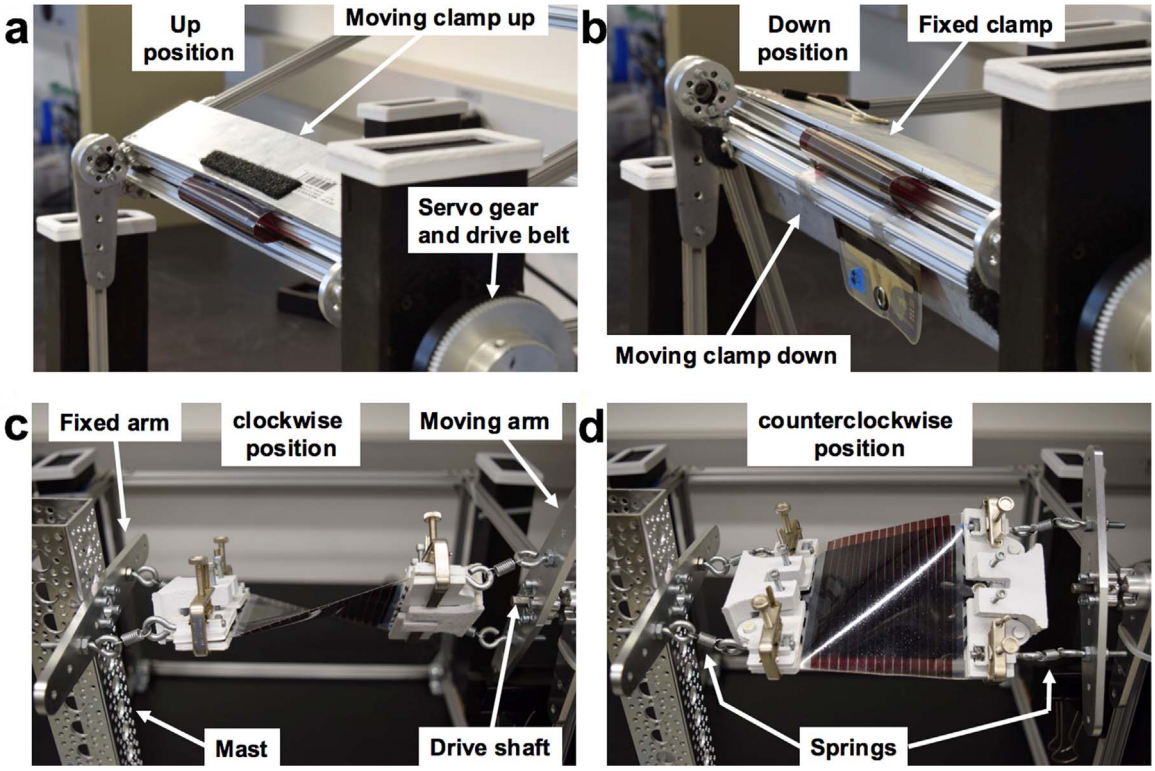

Fig. 2. The purpose-built mechanical testing apparatus used in the study. For the bending mode, (a) indicates the end position of the upward movement and (b) indicates the end position of the downward movement. For the torsion mode, (c) shows the end position of the clockwise movement (from the perspective of the servo gear) and (d) shows the end position of the counterclockwise movement.

accommodate some of the torsional strain so that the modules were not immediately damaged (see Supporting Information for spring/clamp configuration for each module type). Both modules experienced 35° of angular displacement in each direction despite the fact that their differing thicknesses made different springs necessary for the modules to survive thousands of torsional cycles before failing. We therefore believe that the springs accommodated most, but not all, of the additional strain beyond what we calculated for a 35° angular displacement and this implies that the actual maximum shear stress was slightly higher than the calculated value. Ultimately, we take the fact that the calculated torsional stress was two orders of magnitude below yield for oPET, along with the ability of the modules to withstand multiple torsional cycles before rupture, as proof that the shear strain during torsion was in the elastic regime.

4. Experimental methods

4.1. Preparation of modules

Prior to mechanical testing, both "test" and "control" modules were exposed to AM1.5G simulated solar irradiance at 1000 W/m^2 in a solar simulator (ABET Sun 2000) for a burn-in period of 80 min. We took this step to stabilize the performance of the modules and to separate their decline from aging from that caused by mechanical degradation [26]. Control modules were used to isolate effects of mechanical degradation from the possible modes of non-mechanical degradation (i.e. photochemical degradation) over time. The current-voltage properties of one undeformed control module were measured for each deformed module before testing began and after each interval of mechanical testing.

4.2. Construction of apparatus for cyclic loading

The OSC modules were tested in the bending mode by a purpose built apparatus utilizing a servo motor (Teknik ClearPath CMPV, Victor, NY) with aluminum trussing (Microrax, Auburn, WA) and structural elements (Actobotics, Winfield, KS.) shown in Fig. 2. The drive train of the step motor was connected to a moving arm to which one end of the rectangular module was clamped. The other end of the device was clamped to a fixed position on the frame of the testing apparatus and pieces of PDMS (120 × 10 × 2 mm) were sandwiched between the aluminum bar clamps and both the top and bottom sides of each end of the device to prevent slippage and to protect the modules from the hard corners of the aluminum clamps. Great care was taken in fixing every device into the machine in the exact same way. After positioning the devices into the apparatus in a rest position, the motor was enabled and the frame moved to its upward position where the bending program was then initiated that sent commands to move ~260° from one position to the other once per second (See Fig. S1 for complete experimental setup). After testing about half of the modules (some surviving more than 30,000 cycles without catastrophic failure) a cutoff of 15,000

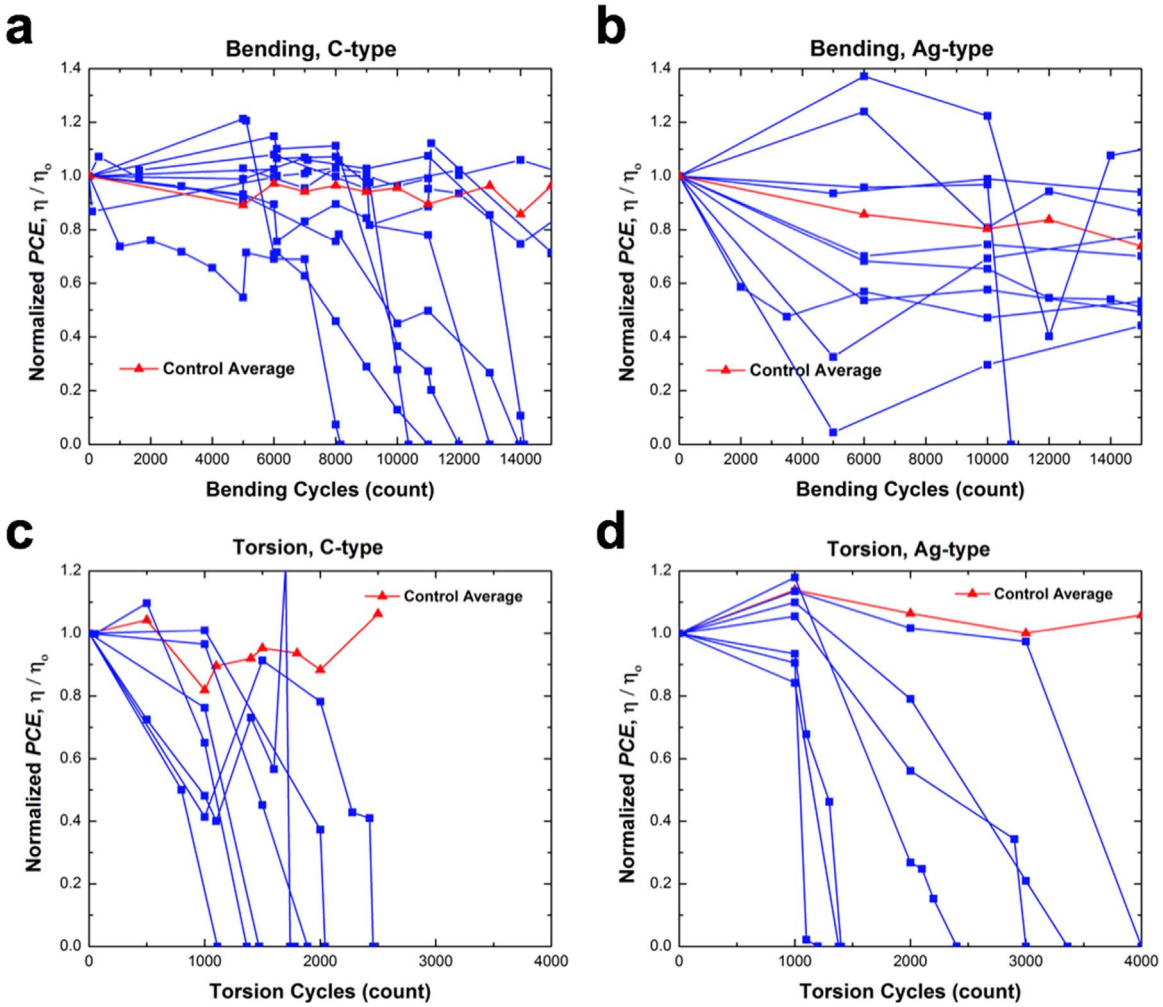

Fig. 3. Graphic results of mechanical testing for bending of (a) C-type and (b) Ag-type modules along with torsion of (c) C-type and (d) Ag-type modules. As stated in the Experimental Methods, the Ag-type modules had stronger springs on the moving side only while the C-type had weaker springs on both the moving and fixed side. That is, the stress was greater for the Ag-type modules, which had a thicker encapsulation barrier while the rotational displacement and resulting strain were approximately the same for each module type.

bending cycles was established since it was impractical to test devices indefinitely.

For the torsion mode, the same apparatus was modified with parts made from machined aluminum and 3D-printed plastic such that the drive axle was mounted with a moving arm to which one end of the device was clamped and connected with springs as shown in Fig. 2. The other end of the device was clamped and connected with springs to a fixed arm connected to a mast at a distance such that the device was suspended horizontally when in a rest position. The size of the springs was chosen to dampen the torsional stress upon the solar cell modules so that they would last for hours under many cycles of stress rather than quickly tearing under the torque generated by the step motor (see Fig. S2 for detailed comparison of the clamp/spring configuration for each module type). Similar to the bending modality, the two end positions of the full torsion movement were actuated through the manufacturers software program for controlling the step motor and a freeware program that sent move commands once per second by automatic clicking of the mouse. One bending or torsion cycle lasted approximately 2 s. The full range of motion for both device types was 70° ± 1° (see Video V2 for C-type torsion and Video V3 for Ag-type torsion).

4.3. Photovoltaic measurements

Photovoltaic performance was measured with a solar simulator (ABET Technologies Sun 2000, Milford, CT) and source meter (Keithley 2400) periodically to generate a plot of current density vs. voltage (*J-V*) throughout the testing period. Due to the time involved in unclamping the device, testing it, and reclamping the device in the apparatus, we established experimentally a “first testing interval” before which there was no damage or decline in device performance. For example, we bend-tested the first several C-type modules and observed that none of the devices exhibited defects before 4000 bending cycles. We therefore began to pause bend testing after 4000 cycles to unclamp the module in order to visually inspect it and take photovoltaic measurements. After this initial number of cycles and subsequent investigation, mechanical testing was halted to take photovoltaic measurements of the test and control samples every few thousand cycles. We continued testing until the modules produced open circuits.

4.4. Finite element analysis

Numerical modeling with the Stress Analysis package in Autodesk Inventor 2016 was used to predict the stresses associated with each type of mechanical testing. Both modules were scaled up to allow for a reasonable mesh size that was amenable to computation. Due to the extremely small thickness of the solar cell device stack in relation to the barrier foil thickness, all modules were simplified to a rectangle composed purely of PET with the modulus edited to that of Mylar 800 oPET as given by the commercial vendor. For the modeling of both bending and torsion, the clamps were composed of aluminum 4000 and were positioned with the clamp on one side in fixed constraint and both clamps in their proper positions with respect to the OSC modules. Over the course of mechanical testing, we never observed any slippage of the OSC modules when they were sandwiched between the rectangular sections of PDMS, and for this reason, we specified bonded contacts between the oPET and aluminum clamps. Because the force in each form of mechanical testing is delivered by a drive shaft connected to a stepper motor, the force in the bending FEA model (Fig. 4) consisted of a moment about the transverse axis of the OSC module while in the torsion FEA model (Fig. 6), the moment was about the longitudinal axis. For the bending model, the traditional Von Mises stress revealed the stress concentration near the clamp point but in the case of the torsion model, we found that the in-plane (x-y) stress map more clearly indicated the point at which crack initiation occurred.

5. Results and discussion

As the plots in Fig. 3 show, the C-type modules were more fragile than the Ag-type modules under both bending and torsion. The C-type modules were the first to undergo bending and the testing of ten modules was necessary to produce seven that failed. We therefore tested ten Ag-type modules but only one failed. Due in large part to their lesser tolerance of shear, torsion testing produced failure in seven out of seven OSC modules of both types, although the Ag-type modules were again more resilient. The difference that is most relevant between the C-type and Ag-type modules was their difference in thickness due to the presence of the UV filter in the Ag-type modules. This filter appeared to have the benefit of increasing the mechanical robustness of

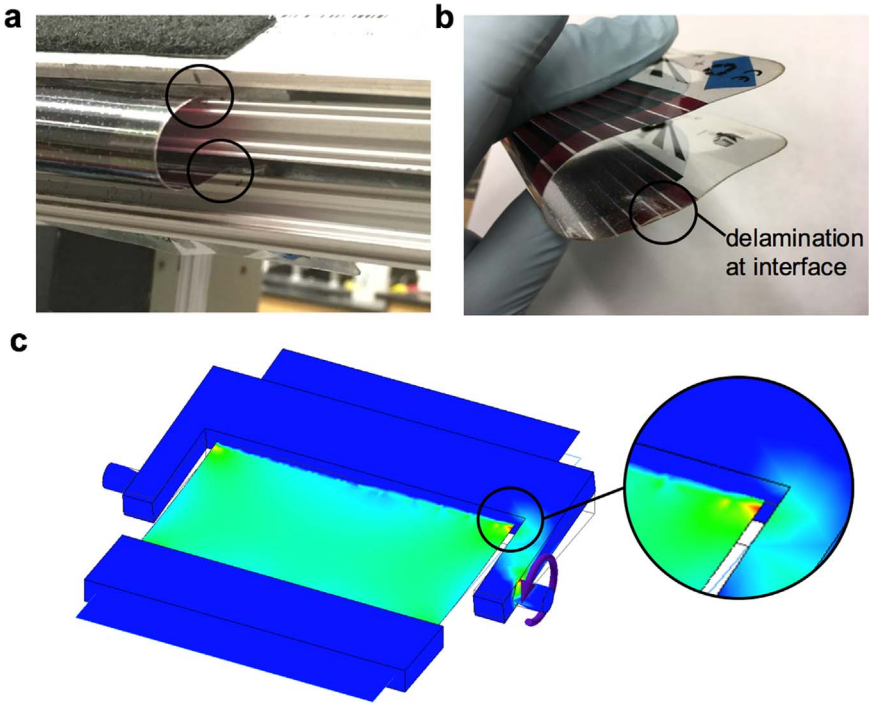

Fig. 4. Photos of the device/clamp interface and delamination of the OSC module. The position in which the moving arm is oriented up is shown in (a) with circles that indicate the interface of PDMS and the OSC module. A representative OSC module is shown in (b) where the circled region indicates delamination that originated at the clamp/device interface. A finite element analysis in (c) shows the Von Mises stress concentration near the clamp/device interface where the inset highlights the origin of delamination.

the Ag-type modules.

5.1. Cyclic bending

5.1.1. Delamination

In the case of bending, the C-type module (surprisingly) experienced no defects in the middle of the module at the apex of the bend. Instead, delamination originated from shear at the ends where it was sandwiched between layers of PDMS and secured to the apparatus (Fig. 4). This delamination typically began after 5000–8000 cycles and then slowly progressed over the course of thousands of bending cycles. This delamination consisted of a splitting of the device stack between the active P3HT layer and the PEDOT:PSS electron-blocking layer. This delamination propagated over the course of thousands of cycles without any apparent penalty in module performance until the delamination spanned about 75% of the width of the module, at which point the modules delaminated more rapidly. All figures of merit declined precipitously during this final phase until eventually culminating in an open circuit due to separation across the entire width of the device stack. Once initiated, catastrophic failure occurred within a few thousand bending cycles. We observed this behavior in seven out of ten modules tested; three modules did not delaminate and were still functioning at the end of the test.

All other testing parameters being fixed, a likely reason for the lack of failure in 30% of the C-type modules is that the individual modules were sectioned from the parent roll with the use of a 90 W CO_2 laser at a speed of 4.5 m s^{-1} that allows for bulk manufacture. It has been asserted that, opposed to shearing the films by cutting them, laser-sectioning allows a superior edge seal that can prevent delamination [27]. There appears to be, however, a lack of uniformity in the rough edges of the device, perhaps due to the speed at which an incomplete melt of the oPET occurs as well as the presence of P3HT:PCBM at the edges from slot-die coating across the entire width of the parent roll. At the edge of each module, there is also the UV-curable adhesive layer that is necessary to bind the laminates together, and the presence of all these molecular constituents and the rapid heating and cooling from laser sectioning makes the microstructure at the edge of the modules lack uniformity. As delamination of these modules began non-preferentially at any of the four edge locations where the module was clamped into the bending apparatus, it could simply be the case that there was not a microstructural defect to act as a center of stress concentration at any of these four edge locations in the three modules that did not delaminate.

In the Ag-type modules, there was no delamination observed in nine out of ten modules before the 15,000-cycle cutoff was reached. Testing was extended for some of these modules to 20,000 cycles with no observable defect or decline in performance. This result suggested that the modules could perhaps be mechanically stable over many more bending cycles than it was practical for us to test. It is notable that the module

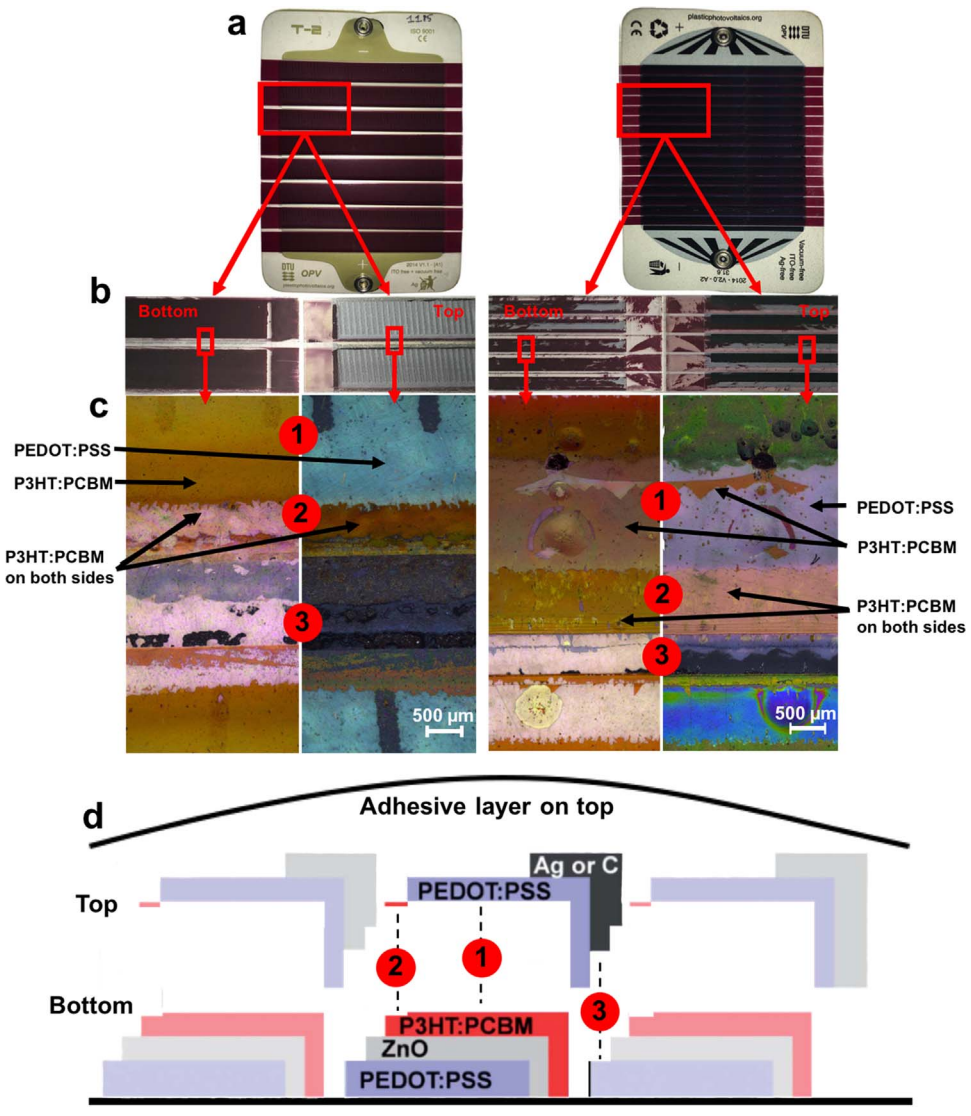

Fig. 5. An investigation of the separation of solar cell module sections after delamination and device failure during cyclic bend testing. From top to bottom, (a) shows the Ag-type and C-type devices where the rectangles indicate the delaminated regions where sample sections shown in (b) were cut out. The rectangles at the sample section level indicate where optical micrographs were taken of two halves of the device that were separated by delamination in (c). In (d), the device stack schematic in Fig. 1 is modified to reflect the separation of layers upon delamination. The numbers in the red circles correlate the three locations shown in top-down view in the micrographs in (c) with the side view schematic in (d) (For interpretation of the references to color in this figure legend, the reader is referred to the web version of this article.).

that failed did so at the apex of the bend and failed rapidly, delaminating audibly and all at once. This difference in mechanical response implies that if the barrier encapsulant is sufficiently thick, it can accommodate the shear at the clamps but may then eventually fail from bending stress at the apex.

5.1.2. Crazing

During testing, we took optical micrographs at the suspected regions where delamination would occur and then examined those same regions again along with the periodic photovoltaic measurements as testing progressed. From these images, we determined that the underlying cause of the delamination appeared to be the formation of crazes, which are porous regions of plastic deformation in a glassy polymer (and some semicrystalline polymers such as the oPET)resembling cracks that develop at rough edges of stress concentration [28,29]. Furthermore, studies have shown that craze formation occurs at the tip of crack formation in polymers and over the course of this study, we repeatedly observed craze formation preceding both delamination (upon bending) and tearing (upon torsion) [30]. Because craze matter has a different index of refraction than that of the bulk polymer, it is easily visible under optical microscopy.

5.2. Cyclic torsion

5.2.1. Tearing

In the case of torsion, we found that by selecting the proper spring thickness and angular rotation of the drive axle it was possible to tune the testing apparatus to an ideal angular displacement that did not quickly tear the module nor allow it to survive undamaged for a prohibitive period of time. In the case of the Ag-type modules, the fixed end was connected directly to the stationary modules without a spring to dampen torsional stress, while the carbon electrode modules had dampening springs connected to both the stationary and moving arms (as shown in Fig. 2). This was necessary because the torsion that was required to shear the Ag-type modules to eventual failure exceeded the fracture strength of the C-type modules and would immediately tear them.

Proper tuning for each module type, along with the lesser resistance of the barrier foil to shear, resulted in a 100% failure rate for $n = 7$ devices. As Fig. 3 shows, the Ag-type modules were slightly more resistant to torsion than the C-type modules, even without springs on the fixed end, again presumably due to the increased thickness of the barrier foil. Within the range of hundreds to a few thousand cycles, a small tear would occur approximately 1–2 cm from the edge of the moving clamp, roughly corresponding to the edge of the diagonal creases that would develop in the module as it was twisted. In both types of module, open circuit failure from the module being torn in two pieces generally occurred within a few thousand cycles after the initial formation of a crack. A notable exception to this behavior was one of the Ag-type modules, which, instead of tearing, delaminated across much of the module (as opposed to local delamination as observed during bending) to relieve strain. As we observed with modules under bending, we also observed craze formation leading to cracking with modules under torsion. Rather than propagating transversely across the module leading the delamination front (as with bend testing), under torsion, crazes during torsion were observed oriented 45–60° to the direction of crack (tear) propagation (Fig. 6).

5.3. Delamination and separation of the device stack

The path of delamination was examined by optical microscopy (Fig. 5). For each of the module types, the majority of the P3HT:PCBM appears to have stayed with the bottom half of the module (the side facing incident light according to Fig. 1) when the two halves were torn apart during delamination. In the photographs of the separated sections (Fig. 5b), the rosy coloration on each of the top halves near the edges of

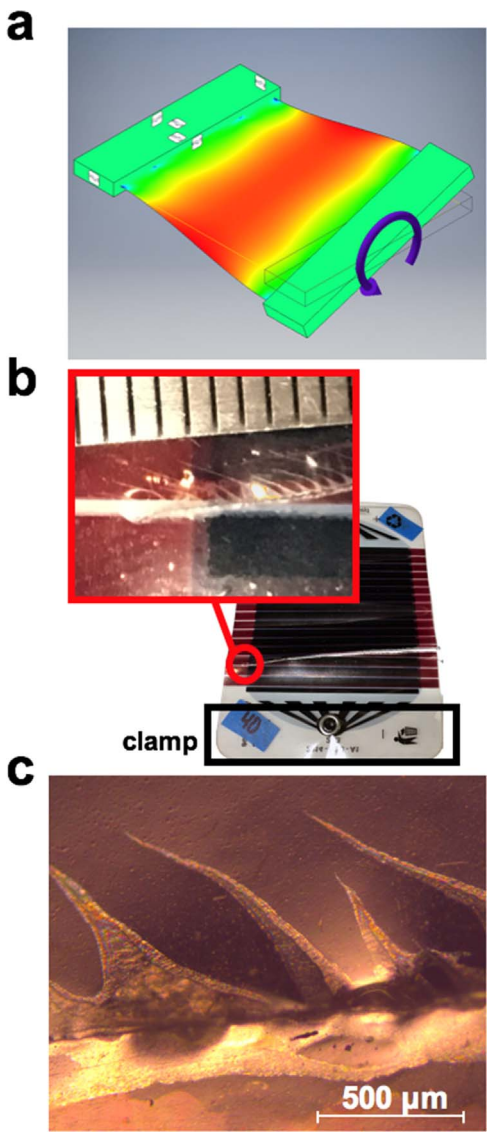

Fig. 6. Finite element analysis and prediction (FEA) and resulting tearing of C-type module under torsion. (a) Shows an FEA map of shear stress in the plane of the device. A representative module after open circuit in (b) shows the tear path with the inset providing a close-up view of the crack tip next to millimeter gradations on a ruler. An optical micrograph in (c) shows the crazing around the tear.

the module indicate that some decohesion of P3HT:PCBM did occur presumably due to the adhesive layer that covers the top side of the module. This decohesion, where the P3HT:PCBM layer was torn apart, leaving some active material stuck to the adhesive on one side while the rest separated with the other side, is also evident in the micrographs of the separated sections of the module (Fig. 5c, location 2). This observation is unsurprising because the slot die coating of P3HT:PCBM extends all the way to the edge of each module while the rest of the layers were printed with approximately 10 mm margins. The notoriously poor cohesive energy of the P3HT:PCBM active layer made it susceptible to separation when delamination began at the edges [5]. When this delamination reached the rest of the device stack, however, the primary plane of separation was the interface between the P3HT:PCBM and PEDOT:PSS, as indicated by the clear separation of orange and blue (Fig. 5c, location 1). This result was expected because it has been reported that the interface between these two materials was the weakest interface within the device stack [6].

As a consequence of the staggered layout of printed layers necessary for the serial electrical connectivity within the module, the horizontal

plane of delamination separated at whichever interface had the weakest adhesion (Fig. 5d). Thus, while P3HT:PCBM decohered where that layer was in contact with the adhesive top layer (Fig. 5d, location 2), the P3HT:PCBM and top PEDOT:PSS layers delaminated where they were in contact (Fig. 5d, location 1). The carbon and silver nanoparticle electrode materials separated from the bottom PEDOT:PSS layer on a lower plane than the P3HT:PCBM/adhesive and P3HT: PCBM/PEDOT:PSS interfaces (Fig. 5c-d, location 3). Additionally, the coloration in the micrographs of separated module halves indicates that the top PEDOT:PSS layer, where it is not in contact with P3HT:PCBM, instead separated from the underlying barrier substrate in the C-type module and to a lesser extent in the Ag-type module (Fig. 5c-d, location 3).

In the case of torsion, the deformation surrounding the tear was so localized that cutting out the region in question for examination was not possible without further damaging the sample in the torn region. It appeared, however, that separation of layers in the device stack was not as relevant in this mechanical mode, as shear stress in both module types led to craze formation within as few as 10 cycles and crack propagation within 50–2000 cycles until all modules tested were torn completely apart. As Fig. 3 shows, no module lasted longer than 4000 cycles. The slightly longer fatigue life for the Ag-type modules was likely the result of their slightly thicker barrier foil. An example of a representative C-type module is shown in Fig. 5 accompanied by a finite element analysis color map showing how the shear strain contours agree with the site of crack initiation.

6. Conclusion

We have demonstrated that roll-to-roll printed OSC modules are able to withstand thousands of cycles of bending and torsion. The lifetime against fatigue of these modules is dependent upon the thickness of the encapsulation barrier, as this is the most durable material in the device stack. Primary causes of mechanical failure are crazing that originates at centers of stress concentration on the rough outside edges of the laser-cut oPET/SiO_2 barrier foil, and shear forces generated at the grips in bending deformations. We conclude that the modules considered here are sufficiently robust for normal roll-to-roll coating and significant—though not extreme—degrees of cyclic deformation. For significant deformations and longer cycling, for example solar blankets, tarps, textiles, and wearable devices [11], the mechanical robustness will need to be improved. In particular, this report points to a need to improve sealing processes (i.e., laser cutting) and the toughness of the foils used for substrates and encapsulants. Damage originating from cohesive or adhesive failure of the active materials can be addressed by engineering the molecular structure [1], molecular weight [31,32], or morphology [33] of the organic semiconductors. In any case, we assert that OSC modules represent the photovoltaic technology with the greatest potential for extreme—and repeated—mechanical deformation.

Acknowledgements

This work was supported in part by the Air Force Office of Scientific Research (AFOSR), grant number FA9550-16-1-0220. Additional support was provided by the National Science Foundation Graduate Research Fellowship under grant number DGE-1144086 awarded to A. V. Z. This work was performed in part at the San Diego Nanotechnology Infrastructure (SDNI), a member of the National Nanotechnology Coordinated Infrastructure, which is supported by the National Science Foundation (Grant ECCS-1542148).

Appendix A. Supporting information

Supplementary data associated with this article can be found in the online version at http://dx.doi.org/10.1016/j.solmat.2017.08.015.

References

[1] S. Savagatrup, A.D. Printz, T.F. O'Connor, A.V. Zaretski, D. Rodriquez, E.J. Sawyer, K.M. Rajan, R.I. Acosta, S.E. Root, D.J. Lipomi, Mechanical degradation and stability of organic solar cells: molecular and microstructural determinants, Energy Environ. Sci. 8 (2015) 55–80, http://dx.doi.org/10.1039/C4EE02657H.
[2] M.O. Reese, S.A. Gevorgyan, M. J??rgensen, E. Bundgaard, S.R. Kurtz, D.S. Ginley, D.C. Olson, M.T. Lloyd, P. Morvillo, E.A. Katz, A. Elschner, O. Haillant, T.R. Currier, V. Shrotriya, M. Hermenau, M. Riede, K.R. Kirov, G. Trimmel, T. Rath, O. Ingan??s, F. Zhang, M. Andersson, K. Tvingstedt, M. Lira-Cantu, D. Laird, C. McGuiness, S. Gowrisanker, M. Pannone, M. Xiao, J. Hauch, R. Steim, D.M. Delongchamp, R. R??sch, H. Hoppe, N. Espinosa, A. Urbina, G. Yaman-Uzunoglu, J.B. Bonekamp, A.J.J.M. Van Breemen, C. Girotto, E. Voroshazi, F.C. Krebs, Consensus stability testing protocols for organic photovoltaic materials and devices, Sol. Energy Mater. Sol. Cells 95 (2011) 1253–1267, http://dx.doi.org/10.1016/j.solmat.2011.01.036.
[3] F.C. Krebs, T.D. Nielsen, J. Fyenbo, M. Wadstrøm, M.S. Pedersen, Manufacture, integration and demonstration of polymer solar cells in a lamp for the "Lighting Africa" initiative, Energy Environ. Sci. 3 (2010) 512, http://dx.doi.org/10.1039/b918441d.
[4] A.D. Printz, D.J. Lipomi, Competition between deformability and charge transport in semiconducting polymers for flexible and stretchable electronics, Appl. Phys. Rev. 3 (2016), http://dx.doi.org/10.1063/1.4947428.
[5] V. Brand, C. Bruner, R.H. Dauskardt, Cohesion and device reliability in organic bulk heterojunction photovoltaic cells, Sol. Energy Mater. Sol. Cells 99 (2012) 182–189, http://dx.doi.org/10.1016/j.solmat.2011.11.035.
[6] S.R. Dupont, M. Oliver, F.C. Krebs, R.H. Dauskardt, Interlayer adhesion in roll-to-roll processed flexible inverted polymer solar cells, Sol. Energy Mater. Sol. Cells 97 (2012) 171–175, http://dx.doi.org/10.1016/j.solmat.2011.10.012.
[7] R. Roesch, T. Faber, E. Von Hauff, T.M. Brown, M. Lira-Cantu, H. Hoppe, Procedures and practices for evaluating thin-film solar cell stability, Adv. Energy Mater. 5 (2015) 1–24, http://dx.doi.org/10.1002/aenm.201501407.
[8] F.C. Krebs, Fabrication and processing of polymer solar cells: a review of printing and coating techniques, Sol. Energy Mater. Sol. Cells 93 (2009) 394–412, http://dx.doi.org/10.1016/j.solmat.2008.10.004.
[9] H. Youn, H.J. Park, L.J. Guo, Organic photovoltaic cells: from performance improvement to manufacturing processes, Small 11 (2015) 2228–2246, http://dx.doi.org/10.1002/smll.201402883.
[10] C.C. Chen, W.H. Chang, K. Yoshimura, K. Ohya, J. You, J. Gao, Z. Hong, Y. Yang, An efficient triple-junction polymer solar cell having a power conversion efficiency exceeding 11%, Adv. Mater. 26 (2014) 5670–5677, http://dx.doi.org/10.1002/adma.201402072.
[11] T.F. O'Connor, A.V. Zaretski, S. Savagatrup, A.D. Printz, C.D. Wilkes, M.I. Diaz, E.J. Sawyer, D.J. Lipomi, Wearable organic solar cells with high cyclic bending stability: materials selection criteria, Sol. Energy Mater. Sol. Cells 144 (2016) 438–444, http://dx.doi.org/10.1016/j.solmat.2015.09.049.
[12] M.S. White, M. Kaltenbrunner, E.D. Głowacki, K. Gutnichenko, G. Kettlgruber, I. Graz, S. Aazou, C. Ulbricht, D.A.M. Egbe, M.C. Miron, Z. Major, M.C. Scharber, T. Sekitani, T. Someya, S. Bauer, N.S. Sariciftci, Ultrathin, highly flexible and stretchable PLEDs, Nat. Photonics 7 (2013) 811–816, http://dx.doi.org/10.1038/nphoton.2013.188.
[13] T. Kim, J.-H. Kim, T.E. Kang, C. Lee, H. Kang, M. Shin, C. Wang, B. Ma, U. Jeong, T.-S. Kim, B.J. Kim, Flexible, highly efficient all-polymer solar cells, Nat. Commun. 6 (2015) 8547, http://dx.doi.org/10.1038/ncomms9547.
[14] U. Lang, N. Naujoks, J. Dual, Mechanical characterization of PEDOT:PSS thin films, Synth. Metals 159 (2009) 473–479, http://dx.doi.org/10.1016/j.synthmet.2008.11.005.
[15] C.M. Stafford, C. Harrison, K.L. Beers, A. Karim, E.J. Amis, M.R. VanLandingham, H.C. Kim, W. Volksen, R.D. Miller, E.E. Simonyi, A buckling-based metrology for measuring the elastic moduli of polymeric thin films, Nat. Mater. 3 (2004) 545–550, http://dx.doi.org/10.1038/nmat1175.
[16] C.M. Stafford, B.D. Vogt, C. Harrison, D. Julthongpiput, R. Huang, Elastic moduli of ultrathin amorphous polymer films, Macromolecules 39 (2006) 5095–5099, http://dx.doi.org/10.1021/ma060790i.
[17] J.-H. Kim, A. Nizami, Y. Hwangbo, B. Jang, H.-J. Lee, C.-S. Woo, S. Hyun, T.-S. Kim, Tensile testing of ultra-thin films on water surface, Nat. Commun. 4 (2013) 2520, http://dx.doi.org/10.1038/ncomms3520.
[18] S.R. Dupont, F. Novoa, E. Voroshazi, R.H. Dauskardt, Decohesion kinetics of PEDOT:PSS conducting polymer films, Adv. Funct. Mater. 24 (2014) 1325–1332, http://dx.doi.org/10.1002/adfm.201302174.
[19] C. Bruner, F. Novoa, S. Dupont, R. Dauskardt, Decohesion kinetics in polymer organic solar cells, ACS Appl. Mater. Interfaces 6 (2014) 21474–21483, http://dx.doi.org/10.1021/am506482q.
[20] P.G. Charalambides, H.C. Cao, J. Lund, A.G. Evans, Development of a test method for measuring the mixed mode fracture resistance of bimaterial interfaces, Mech. Mater. 8 (1990) 269–283, http://dx.doi.org/10.1016/0167-6636(90)90047-J.
[21] G.A. Dos Reis Benatto, B. Roth, M.V. Madsen, M. Hösel, R.R. Søndergaard, M. Jørgensen, F.C. Krebs, Carbon: the ultimate electrode choice for widely distributed polymer solar cells, Adv. Energy Mater. 4 (2014) 1–6, http://dx.doi.org/10.1002/aenm.201400732.
[22] M. Hösel, D. Angmo, R.R. Søndergaard, G.A. dos Reis Benatto, J.E. Carlé, M. Jørgensen, F.C. Krebs, High-volume processed, ITO-free superstrates and substrates for roll-to-rollroll-to-roll development of organic electronics, Adv. Sci. (2014) 1–12, http://dx.doi.org/10.1002/advs.201400002.
[23] B. Roth, G.A. Dos Reis Benatto, M. Corazza, R.R. Søndergaard, S.A. Gevorgyan, M. Jørgensen, F.C. Krebs, The critical choice of PEDOT:PSS additives for long term

stability of roll-to-roll processed OPVs, Adv. Energy Mater. 5 (2015), http://dx.doi.org/10.1002/aenm.201401912.
[24] B. Roth, G.A. dos Reis Benatto, M. Corazza, J.E. Carl??, M. Helgesen, S.A. Gevorgyan, M. J??rgensen, R.R. S??ndergaard, F.C. Krebs, Improving the operational stability of PBDTTTz-4 polymer solar cells modules by electrode modification, Adv. Eng. Mater. (2015) 1–7, http://dx.doi.org/10.1002/adem.201500361.
[25] T.T. Larsen-Olsen, R.R. Søndergaard, K. Norrman, M. Jørgensen, F.C. Krebs, All printed transparent electrodes through an electrical switching mechanism: a convincing alternative to indium-tin-oxide, silver and vacuum, Energy Environ. Sci. 5 (2012) 9467, http://dx.doi.org/10.1039/c2ee23244h.
[26] J. Kong, S. Song, M. Yoo, G.Y. Lee, O. Kwon, J.K. Park, H. Back, G. Kim, S.H. Lee, H. Suh, K. Lee, Long-term stable polymer solar cells with significantly reduced burn-in loss, Nat. Commun. 5 (2014) 1–8, http://dx.doi.org/10.1038/ncomms6688.
[27] F.C. Krebs, M. Hösel, M. Corazza, B. Roth, M.V. Madsen, S.A. Gevorgyan, R.R. Søndergaard, D. Karg, M. Jørgensen, Freely available OPV-The fast way to progress, Energy Technol. 1 (2013) 378–381, http://dx.doi.org/10.1002/ente.201300057.
[28] O.V. Arzhakova, A.A. Dolgova, L.M. Yarysheva, A.L. Volynskii, N.F. Bakeev, Specific features of the environmental crazing of poly(ethylene terephthalate) fibers, Polymer 56 (2015) 256–262, http://dx.doi.org/10.1016/j.polymer.2014.11.044.
[29] I.M. Harris, J.S. Ward, Crazing behaviour in oriented poly(ethylene terephthalate), J. Mater. Sci. 5 (1970) 573–579.
[30] R.P. Kambour, Mechanism of fracture in glassy polymers. III. Direct observation of the craze aheadof the propagating crack in poly(methyl methacrylate) and polystyrene, J. Polym. Sci. Part A-2 4 (1966) 349–358.
[31] C. Bruner, R. Dauskardt, Role of Molecular Weight on the Mechanical Device Properties of Organic Polymer Solar Cells, 2013.
[32] D. Rodriquez, J.-H. Kim, S.E. Root, Z. Fei, P. Boufflet, M. Heeney, T.-S. Kim, D.J. Lipomi, Comparison of methods for determining the mechanical properties of semiconducting polymer films for stretchable electronics, ACS Appl. Mater. Interfaces 9 (2017) 8855–8862, http://dx.doi.org/10.1021/acsami.6b16115.
[33] S.E. Root, N. Jackson, S. Savagatrup, G. Arya, D.J. Lipomi, Modelling the morphology and thermomechanical behaviour of low-bandgap conjugated polymers and bulk heterojunction films, Energy Environ. Sci. 10 (2016) 558–569, http://dx.doi.org/10.1039/C6EE03456J.